International Journal of Marine Engineering Innovation and Research, Vol. 9(4), Dec. 2024. 834-842
(pISSN: 2541-5972, eISSN: 2548-1479)

Analysis of Blade Profile Effects on Performance of Wells Turbine as Wave Energy Converter using CFD Method

Muhammad Anis Mustaghfirin[1], Niki Veranda Agil Permadi[2], Jeheskiel Surbakti[3]
(Received: 31 October 2024 / Revised: 10 November 2024 /Accepted: 25 November 2024 / Available Online: 31 December 2024)

***Abstract*— An oscillating water column (OWC) is a type of power generation device that converts ocean wave energy into electrical energy. The motion of ocean waves forces air through the OWC column and drives a rotor connected to a generator to produce electricity. The Wells turbine is a typical kind of rotor for OWC system. The performance of the Wells turbine can be influence by various factor, such as its geometry. Over the time, various research have been conducted to enhance the Wells turbine design. This study aims to analyze the impact of blade profiles on an 8-bladed Wells turbine's performance using the Computational Fluid Dynamics (CFD) method. A full-domain with multiple reference frame (MRF) approach is applied to represent the rotating flow of the turbine. The flow is solved using Reynold Average Navier-Stokes (RANS) solver accompanied by shear stress transport ($k-\omega$ SST) turbulunce model to capture the boundary layer near the wall. In this study, some blade profiles including NACA 0012, NACA 0015, and NACA 0018, with chord lengths of 100 mm, 125 mm, and 150 mm, are examined. The results of this study reveal that the NACA 0018 blade profile with a 150 mm chord length improves the torque coefficient (C_T) by 36.28% and the power coefficient (C_P) by 1.04% compared to other configurations.**

Keywords—Incompressible Flow, OpenFOAM, OWC, Power Coefficient, RANS, Torque Coefficient, Wells Turbine

I. INTRODUCTION

Ocean wave energy is among the most sustainable resources because it provides a clean and environmentally acceptable substitute to fossil fuels. At appropriate locations, it can generate power up to 90%. The ocean wave energy seems intriguing. It has been studied by researchers over the past two decades due to its potential of prominent energy density and long-lasting availability [1].

In recent decades, several investigations have focused on wave energy converters (WECs) and associated technologies [2], [3]. One of the most favorable wave energy converters is the ocean water column (OWC). By far the popular wave energy device is the OWC, which is simple to use. There are numerous OWC devices have been already deployed in the sea [4]. The OWC employs an air turbine e.g. Wells turbine to convert flow's kinetic energy into mechanical energy [5].

The Wells turbine is a type of air turbine that has staggered radially at 90-degree angles. It operates efficiently in bidirectional airflow without needing to change the direction of the blades or reverse their orientation. The Wells turbine has various limitations including its lower aerodynamic efficiency, high noise levels, narrow operating range, poorer starting characteristics, and high axial force. Therefore, several research have been conducted to enhance the Wells turbine design over time [5].

Wells turbine performance can be influence by various factor, such as the geometry itself. Some related studies had been conducted to examine the performance of Wells turbine using experimental study or numerical method.

Kim et al analyzed the impact of geometry of Wells turbine with NACA0020 installed and accompanied by different hub-tip ratio using CFD. The simulation was only performed on single blade with periodic boundary condition [6]**.** The study showed that the hub-to-tip ratio of 0.7 provides optimum performance. Other related study was conducted by Takao et al. [7]. The study indicated that NACA0015 blade profile is the best suited for the substantial Wells turbine. However, NACA0021 blade profile provides superior performance in the post-stall regime than NACA0015 [8].

An experiment conducted by Takao et al. [9] showed that as the blade thickness increases the torque coefficient decreases in the region of flow coefficient which is smaller than stall point. However, when the blade is altered to a non-parallel distribution (3D-blde), the toque coefficient increases.

Although the development of Wells turbine is well-performed by experiment, computational fluid dynamics (CFD) have become favorable for design optimization [10]. The computational fluid dynamic (CFD) is often utilized to solve the flow field and provide the

[1]Muhammad Anis Mustaghfirin, Department of Marine Engineering, Shipbuilding Institute of Polytechnic Surabaya, Surabaya, 60111, Indonesia. Email: niki.veranda@ppns.ac.id
[2]Niki Veranda Agil Permadi, Department of Marine Engineering, Shipbuilding Institute of Polytechnic Surabaya, Surabaya, 60111, Indonesia. Email: niki.veranda@ppns.ac.id
[3]Jeheskiel Surbakti, Department of Marine Engineering, Shipbuilding Institute of Polytechnic Surabaya, Surabaya, 60111, Indonesia. Email: niki.veranda@ppns.ac.id

performance characteristic of Wells turbine in more efficient way compared to experiment. The CFD is mainly performed using numerical method. Some key techniques that influence the accuracy of CFD simulation are mesh generation, numerical schemes, and turbulence modelling. Reynolds Average Navier-Stokes (RANS) solved by Semi-Implicit Method for Pressure Linked Equations-Consistent (SIMPLEC) algorithm and coupled with shear stress transport ($k-\omega\ SST$) turbulence model is frequently used for the simulation of Wells turbine [8], [11], [12], [13], [14].

In analyzing rotating motion, meshing techniques are crucial for accurately representing the flow around a rotating body. Kotb et al. [15] employed CFD and a multi-objective genetic algorithm (MOGA) to optimize the operational range of a Wells turbine. The study focused on an 8-bladed Wells turbine, with only one blade meshed and periodic boundary conditions applied to the fluid domain assuming that each blade encounters identical flow conditions. The result indicated an 18.23% increase in turbine efficiency at flow coefficient (φ) of 0.225. The CFD technique in this study also yielded accurate results when compared to experimental data. In related studies, Kotb et al. [16], [17] simulated the Wells turbine by varying the tip clearance and adding a tapered leading-edge micro cylinder. ANSYS Fluent software was used with an unstructured mesh and a skewness correction factor of 1. The simulation approach demonstrated accuracy in predicting the performance of the new Wells turbine design. Next, Uddin et al. [18] conducted a CFD study on a hybrid Wells turbine that combined NACA 0015 and NACA 0025 airfoil profiles. The investigation utilized a single-blade domain with periodic boundary conditions, based on the assumption of symmetric flow. The domain was discretized using an unstructured mesh in ANSYS software, and the results demonstrated strong agreement with experimental data. In a related study, Wang et al. [19] also used ANSYS but employed a mapped hexahedral (map-hex) mesh for the entire fluid domain. The numerical model validation showed high accuracy when compared with experimental results.

Most CFD simulations of the Wells turbine utilize only a single blade with periodic boundary conditions, under the assumption that each blade experiences identical flow conditions. This approach effectively reduces computational costs. However, the use of periodic boundary conditions neglects the wake interactions between blades, which are present in an actual Wells turbine. In reality, each blade interacts with the wakes of neighbouring blades, influencing blade loading and overall turbine performance. Consequently, this simplified approach may not fully capture the individual behaviour of each blade.

To address these limitations, this study aims to simulate the Wells turbine with a fully discretized blade model, allowing for a more precise analysis of how specific design parameters, such as blade profiles and chord length, influence turbine performance. This study represents the Wells turbine's real-world operating conditions by applying a full-domain simulation with a multiple reference frame (MRF) approach, capturing the true aerodynamic interactions between the blade and incoming flow. This method enables a deeper understanding of the effect of various design parameters on turbine performance.

The simulations in this study are conducted using the open-source CFD software OpenFOAM, known for its extensive development in fluid mechanics applications and its widespread use for Oscillating Water Column (OWC) studies alongside ANSYS Fluent [3]. For the initial design, a NACA 0015 blade profile with a 125 mm chord length was selected, as it has been commonly used in previous studies [12], [20], [21], [22]. Additionally, two other blade profiles, NACA 0012 and NACA 0018, with thicknesses below and above that of NACA 0015, are examined to identify the optimal configuration.

II. METHOD

2.1 Geometry

The initial geometry used in this study is 8-bladed Wells turbine with NACA 0015 profile as shown in Figure 1. The detail specification of the model is summarized in Table 1.

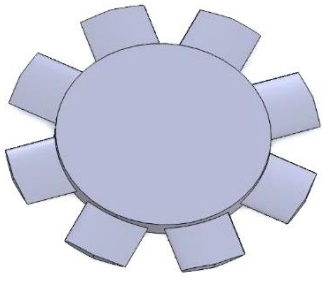

Figure. 1. Initial geometry with NACA 0015

TABLE 1.
INITIAL SPECIFICATION OF THE WELLS TURBINE

Blade profile type	NACA 0015
Number of blades (N_B)	8
Hub Height (H_H)	40 mm
Chord length (C)	125 mm
Hub radius (R_H)	200 mm
Tip radius (R_T)	294 mm
Rotation speed (ω)	2000 rpm

2.2 Simulation Method

$$\boldsymbol{\nu_t = \frac{a_1 k}{max(a_1\omega, SF_2)}} \quad (3)$$

$$\boldsymbol{\frac{\partial k}{\partial t} + U_j \frac{\partial k}{\partial x_j} = P_k - \beta^* k\omega + \frac{\partial}{\partial x_j}\left[(\nu + \sigma_k \nu_t)\frac{\partial k}{\partial x_j}\right]} \quad (4)$$

$$\boldsymbol{\frac{\partial \omega}{\partial t} + U_j \frac{\partial \omega}{\partial x_i} = \alpha S^2 - \beta\omega^2 + \frac{\partial}{\partial x_j}\left[(\nu + \sigma_\omega \nu_t)\frac{\partial \omega}{\partial x_j}\right] + 2(1 - F_1)\sigma_{\omega 2}\frac{1}{\omega}\frac{\partial k}{\partial x_i}\frac{\partial \omega}{\partial x_i}} \quad (5)$$

The finite volume method is used in this research with a steady-state incompressible flow solver. The fluid used in this study is incompressible air under the room temperature of $25°C$. The governing equations of fluid mechanics include the continuity equation and momentum equation. For the incompressible flow, the governing equations can be expressed as Equation (1) and Equation (2).

$$\boldsymbol{\nabla . U = 0} \quad (1)$$

$$\boldsymbol{\frac{\partial U}{\partial t} + \nabla . (UU) = -\frac{\nabla p}{\rho} + \nu \nabla^2 U + f} \quad (2)$$

Where U is the velocity vector, p is the pressure, ν is the fluid kinematic viscosity, and f is the external forces. In this study, no external source is applied. Equation (2) can be decomposed using Reynold decomposition which is also known as Reynold-Averaged Navier-Stokes (RANS) equation. The decomposition process produces an additional term called Reynold stressed which can be solved using turbulence modeling.

In present study, the shear stress transport turbulence model ($k - \omega$ SST) introduced by Menter is used to capture the turbulent flow around the Wells turbine coupled with Spalding wall function [23], [24], [25]. The turbulence kinetic energy k, the specific dissipation rate ω, and the kinematic turbulence viscosity ν_t are given in the following equations.

The computation is performed using *simpleFoam* solver in OpenFOAM which is an open-source CFD codes. In addition, the multiple reference frame (MRF) approach is utilized to represent the rotating flow of the Wells turbine. Then, a grid independence test is carried out to determine the sensitivity of the grid density in providing solution. Two grid configurations are used with y^+ value of 50 and 70, respectively. The whole schematic process of this study is summarized in the flow chart represented in Figure 2.

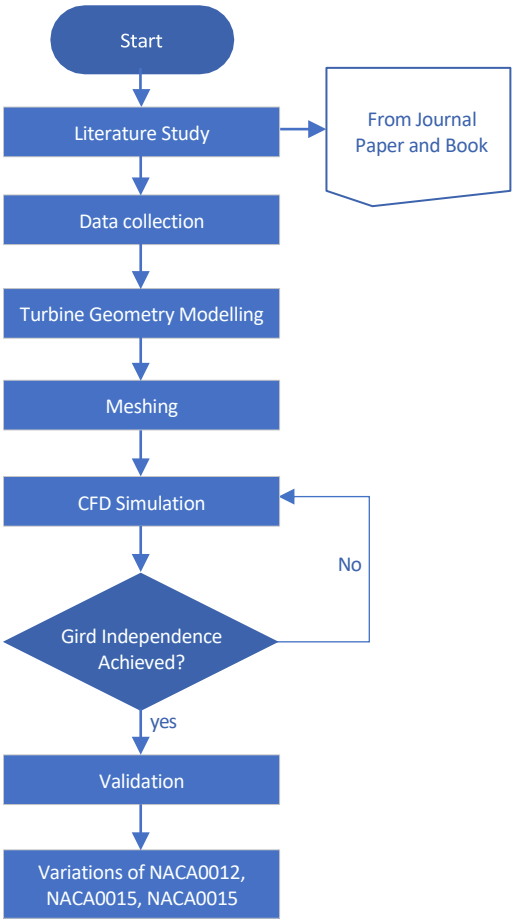

Figure. 2. Flow chart of the simulation

2.3 Computational Domain

The computational domain in this study is a full-domain constructed into cylindrical form. The overall domain length form upstream to downstream is 1500 mm. The left side (upstream) of the domain is assigned as velocity inlet whereas the right side (downstream) of the domain is assigned as outlet pressure. The length of the upstream side and the downstream side are 500 mm (4C) and 1000 mm (8C), respectively. The domain is divided into two regions which are static zone and rotating zone representing the rotational flow caused by the turbine's rotation as shown in Figure 3.

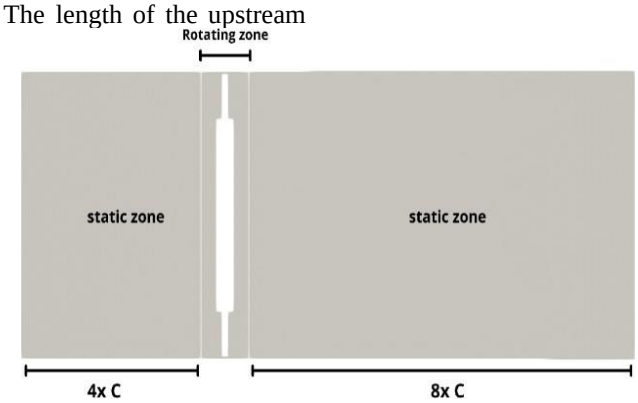

Figure. 3. Computational domain

2.4 Mesh Generation

The fluid domain is discretized into volume mesh using *snappyHexMesh* library in OpenFOAM. The structured mesh was considered with the hex-dominant cell type. The surface triangulation is performed prior to the volume mesh generation to obtained the surface features of the Wells turbine using Salome software. The mesh generation is conducted in two stages. The first stage is the initial mesh which discretizes the computational domain into small cells. Some refinement levels are applied in the rotating zone to capture the rotational flow accurately. The next stage is the inflation layer addition which aims to capture the boundary layer near the turbine model. In this study, 5 layers are generated parallel to the turbine model with the y^+ target of 50 and 70. The result of the meshing process is presented in Figure 4.

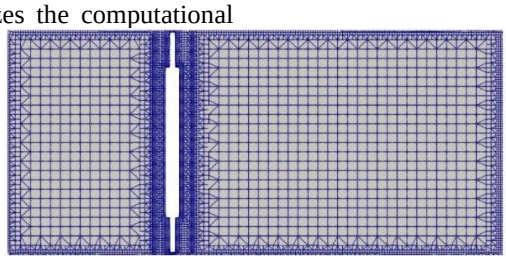

(a)

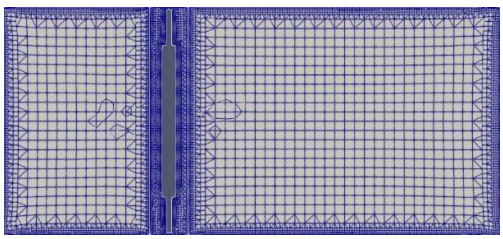

(b)

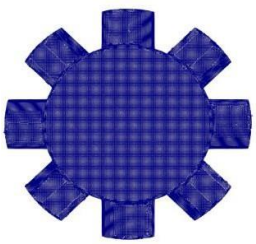

(c)

Figure. 4. (a) Initial mesh; (b) Layered mesh (c) Mesh on turbine’s surface

2.5 Boundary Condition and Numerical Schemes

A fix velocity is imposed on the inlet patch and zero pressure outlet are assigned on the outlet patch. The fluid used is air with room temperature condition. The inlet velocity used in this study is 13.72 m/s. In addition, the turbine's rotation of 2000 rpm is introduced in the rotating zone. The patch name and the boundary conditions for the flow fields in all patches in the domain are presented in Figure 5 and Table 2, respectively. Then, the convective terms and the turbulence properties in the governing equations are discretized using 2nd order schemes linear upwind. As for the gradient terms are solved using cell-based least squares approach.

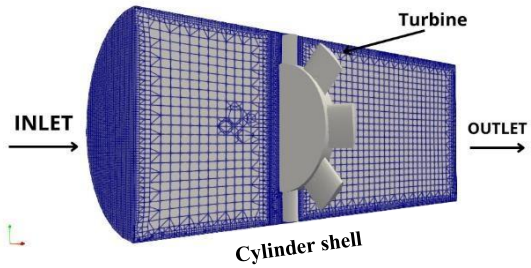

Figure. 5. Patch name in the computational domain

TABLE 2.
BOUNDARY CONDITIONS AT ALL PATCHES

Patch	Type	Boundary conditions	
		U	p
Inlet	Patch	fixedValue	zeroGradient
Outlet	Patch	zeroGradient	fixedValue
Cyl. shell	Wall	noSlip	zeroGradient
Turbine	Wall	movingWallVelocity	zeroGradient

III. RESULTS AND DISCUSSION

3.1 Validation

Validation was performed on two mesh configurations with y^+ values of 50 and 70 with NACA 0015 blade profile. The simulation was carried out at flow coefficient (φ) of 0.225 or equivalent with the axial velocity of 13.72 m/s which is the pre-stall regime. The validation process was designed to determine which mesh configuration yields the most accurate solutions, which were then used to simulate other NACA profiles. Convergence in the simulation was achieved when the torque values stabilized across iterations. Figure 6 illustrates the torque evolution of the NACA 0015 blade profile with a 125 mm chord length, obtained from meshes with y^+ values of 50 and 70. Both meshes demonstrated similar convergence rates. However, in comparison to findings by Kotb et al. [26] the mesh with y^+ 70 slightly underestimated the torque.

The C_T value of the turbine can be calculated with Equation (6)

$$C_T = \frac{T}{\rho \omega^2 R_T^5} \tag{6}$$

where T is the torque value achieved from the simulation, ρ is the air density, ω is the turbine's rotation in rps, and R_T is the tip radius. The result show that the mesh with y^+ 50 yields the most accurate C_T value with a smaller relative error when compared to the study conducted by Kotb et al. as shown in Table 3. The comparison of the C_T value obtained from each mesh is also presented in Figure 7.

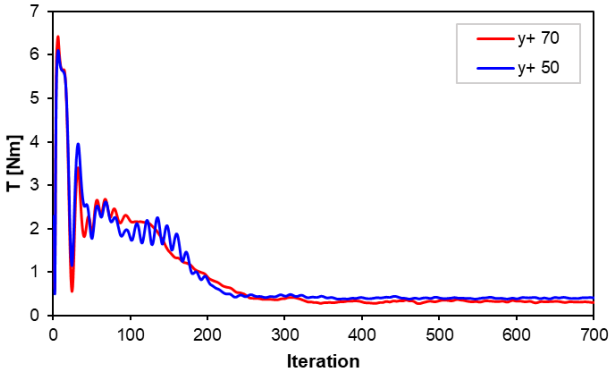

Figure. 6. Patch name in the computational domain

TABLE 3.
COMPARISON OF C_T VALUES WITH OTHER STUDY

Research	Blade Profile	T	C_T	Error (%)
Kotb et al. (2023)	NACA 0015	-	0.128	-
Present study (y^+ 50)	NACA 0015	0.3877	0.132	3.29
Present study (y^+ 70)	NACA 0015	0.3269	0.111	12.89

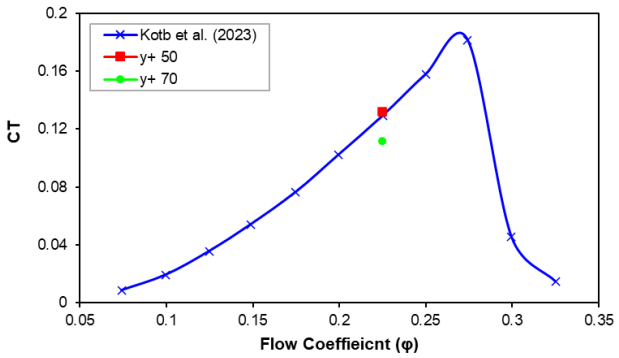

Figure. 7. Comparison of C_T values

3.2 *Performance of Wells Turbine with Various Blade Profiles and Chord Lengths*

This study examines chord lengths of 100, 125, and 150 mm alongside three NACA profiles: 0012, 0015, and 0018. The subsequent analysis focuses on identifying the blade configuration that achieves the highest torque coefficient (C_T) and power coefficient (C_P) values. Figure 8 provides a comparison of each NACA profile at the same chord length.

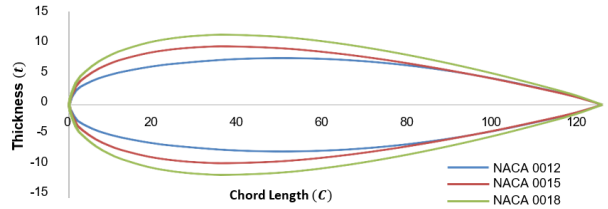

Figure. 8. Comparison of NACA profiles

The torque coefficient (C_T) values vary across different NACA blade profiles and chord lengths. As shown in Figure 9, the torque generated by the NACA 0018 profile increases as the chord length extends from 100 mm to 150 mm. In contrast, the torque values for NACA 0012 and NACA 0015 decrease when a 125 mm chord length is applied. However, these profiles produce significantly higher torque when the chord length is increased to 150 mm. A comparison of all configurations reveals that the NACA 0018 profile with a 150 mm chord length is the most effective at generating torque.

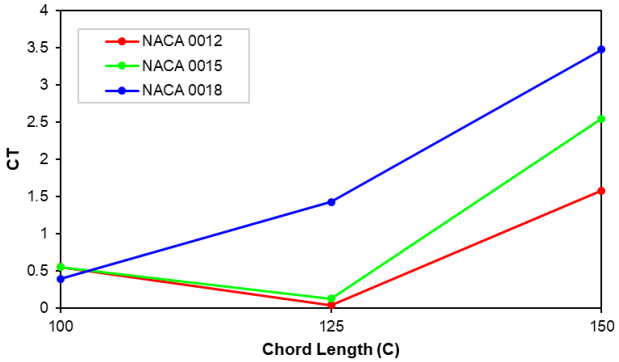

Figure. 9. C_T values of various NACA profiles and chord lengths

In addition to torque coefficient, the power coefficient is also evaluated to obtain the most optimal configuration of Wells turbine. The value of power coefficient (C_P) is expressed in Equation (7).

$$C_P = \frac{\Delta P_0}{\rho \omega^2 R_T^2} \quad (7)$$

where ΔP_0 is the pressure difference between the inlet and outlet of the turbine's flow. Figure 10 depicts the comparison of C_P values provided by various NACA profiles and chord lengths. According to the result, the C_P value increases as the chord length of each blade profile is extended. Furthermore, the result also indicates that NACA 0018 with 150 mm chord length has the highest power coefficient. The Wells turbine's performance with a 150 mm chord length is summarized in Table 4. In the table, the values of $\%C_T$ and $\%C_P$ represent the deviation of the performance compared to the initial design (NACA 0015).

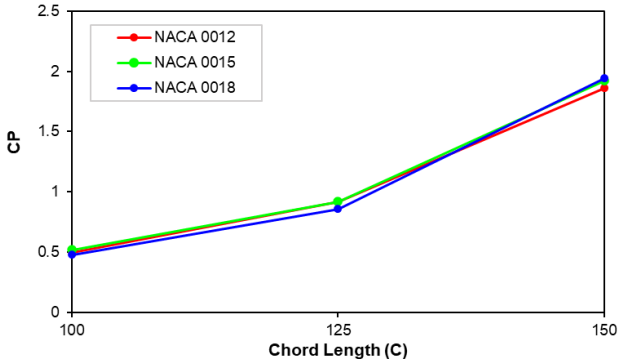

Figure. 10. C_P values of various NACA profiles and chord lengths

TABLE 4.
PERFORMANCE OF WELLS TURBINE WITH VARIOUS BLADE CONFIGURATIONS

Blade Profiles	Chord Length (C)	C_T	C_P	$\%C_T$	$\%C_P$
NACA – 0012	150 mm	1.583	1.86	-37.97	-3.13
NACA – 0015 (initial design)	150 mm	2.552	1.92	-	-
NACA – 0018	150 mm	3.478	1.94	36.28	1.04

3.3 Flow Structures

Figure 11(a), (b), and (c) present the longitudinal velocity contours for NACA 0012, NACA 0015, and NACA 0018 profiles, each with a chord length of 150 mm. Using a fully discretized domain, the simulation effectively captures the interaction between the wakes and individual turbine blades. The results reveal that flow through the turbine is asymmetrical, rather than uniform, which influences the performance of each blade and, consequently, the overall turbine performance.

Additionally, the findings indicate that increasing blade thickness, while maintaining the same chord length, enhances the turbine's ability to extract momentum from the flow more effectively. The result also shows that the flow separation patterns on the suction side are similar across blade profiles. However, as illustrated in Figure 11(a), the NACA 0012 profile is less effective at converting the incoming flow's kinetic energy into mechanical energy compared to NACA 0015 and NACA 0018. This inefficiency is highlighted by a high velocity magnitude in the wake region, indicating greater energy loss. Therefore, NACA 0012 generates a lower torque coefficient than the thicker profiles, NACA 0015 and NACA 0018. Based on this qualitative assessment, NACA 0018 is determined to be the optimal blade configuration.

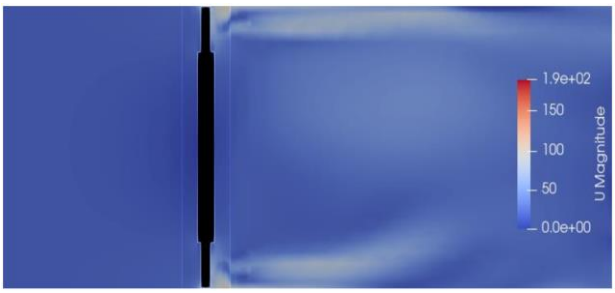

(a)

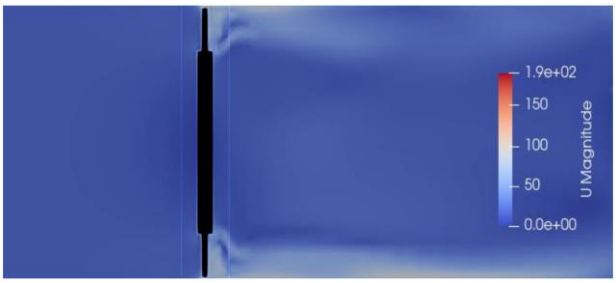

(b)

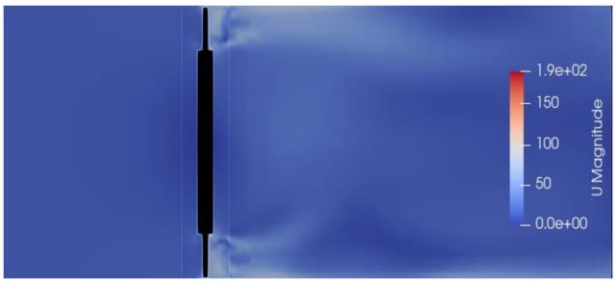

(c)

Figure. 11. Longitudinal velocity contour (a) NACA 0012; (b) NACA 0015; (c) NACA 0018

IV. CONCLUSION

In this research, a CFD method is employed to evaluate the Wells turbine's performance with various blade configurations. A full-domain with MRF approach is applied to represent the rotating flow of the turbine. The Reynold Average Navier-Stokes (RANS) solver is used to solve the flow, accompanied by shear stress transport ($k-\omega$ SST) turbulence model to capture the boundary layer near the wall. In this study, some blade profiles including NACA 0012, NACA 0015, and NACA 0018, with chord lengths of 100 mm, 125 mm, and 150 mm, are examined. The findings in this study conclude that the NACA 0018 blade profile with a 150 mm chord length improves the torque coefficient (C_T) by 36.28% and the power coefficient (C_P) by 1.04% compared to other configurations.

REFERENCES

[1] R. Pelc and R. M. Fujita, "Renewable energy from the ocean," *Mar. Policy*, vol. 26, no. 6, pp. 471–479, Nov. 2002, doi: 10.1016/S0308-597X(02)00045-3.

[2] A. Clément *et al.*, "Wave energy in Europe: current status and perspectives," *Renew. Sustain. Energy Rev.*, vol. 6, no. 5, pp. 405–431, Oct. 2002, doi: 10.1016/S1364-0321(02)00009-6.

[3] F. Opoku, M. N. Uddin, and M. Atkinson, "A review of computational methods for studying oscillating water columns – the Navier-Stokes based equation approach," *Renew. Sustain. Energy Rev.*, vol. 174, p. 113124, Mar. 2023, doi: 10.1016/j.rser.2022.113124.

[4] A. F. O. Falcão and J. C. C. Henriques, "Oscillating-water-column wave energy converters and air turbines: A review," *Renew. Energy*, vol. 85, pp. 1391–1424, Jan. 2016, doi: 10.1016/j.renene.2015.07.086.

[5] M. N. Uddin, F. Opoku, and M. Atkinson, "Investigation of a Modified Wells Turbine for Wave Energy Extraction," *Energies*, vol. 17, no. 15, p. 3638, Jul. 2024, doi: 10.3390/en17153638.

[6] T. Kim, T. Setoguchi, Y. Kinoue, and K. Kaneko, "Effects of blade geometry on performance of wells turbine for wave power conversion," *J. Therm. Sci.*, vol. 10, no. 4, pp. 293–300, Oct. 2001, doi: 10.1007/s11630-001-0035-4.

[7] M. Takao, A. Thakker, R. Abdulhadi, and T. Setoguchi, "Effect of blade profile on the performance of a large-scale Wells turbine for wave-energy conversion," *Int. J. Sustain. Energy*, vol. 25, no. 1, pp. 53–61, Mar. 2006, doi: 10.1080/14786450600593295.

[8] P. M. Kumar and A. Samad, "Effect of Blade Profiles on the performance of Bidirectional Wave Energy Turbine," *MATEC Web Conf.*, vol. 172, p. 06002, 2018, doi: 10.1051/matecconf/201817206002.

[9] M. Takao, K. Takasaki, S. Okuhara, and T. Setoguchi, "Wells turbine for wave energy conversion - improvement of stall characteristics by the use of 3-dimensional blades -," *J. Fluid Sci. Technol.*, vol. 9, no. 3, pp. JFST0052–JFST0052, 2014, doi: 10.1299/jfst.2014jfst0052.

[10] Y. Cui, Z. Liu, X. Zhang, and C. Xu, "Review of CFD studies on axial-flow self-rectifying turbines for OWC wave energy conversion," *Ocean Eng.*, vol. 175, pp. 80–102, Mar. 2019, doi: 10.1016/j.oceaneng.2019.01.040.

[11] Y. Cui and B.-S. Hyun, "Numerical study on Wells turbine with penetrating blade tip treatments for wave energy conversion," *Int. J. Nav. Archit. Ocean Eng.*, vol. 8, no. 5, pp. 456–465, Sep. 2016, doi: 10.1016/j.ijnaoe.2016.05.009.

[12] P. Halder, S. H. Rhee, and A. Samad, "Numerical optimization of Wells turbine for wave energy extraction," *Int. J. Nav. Archit. Ocean Eng.*, vol. 9, no. 1, pp. 11–24, Jan. 2017, doi: 10.1016/j.ijnaoe.2016.06.008.

[13] N. Abdul Settar, S. Sarip, and H. M. Kaidi, "Computational Fluid Dynamics Model of Wells Turbine for Oscillating Water Column System: A Review," *J. Phys. Conf. Ser.*, vol. 2053, no. 1, p. 012013, Oct. 2021, doi: 10.1088/1742-6596/2053/1/012013.

[14] Z. G. Gunawan and Sutardi, "Comparative Numerical Study of Conventional and Hydraulic Wells Turbine for Ocean-Wave Energy Conversion," *BIO Web Conf.*, vol. 89, p. 10001, 2024, doi: 10.1051/bioconf/20248910001.

[15] A. T. M. Kotb, M. A. A. Nawar, Y. A. Attai, and M. H. Mohamed, "Performance optimization of a modified Wells turbine for wave energy conversion," *Ocean Eng.*, vol. 280, p. 114849, Jul. 2023, doi: 10.1016/j.oceaneng.2023.114849.

[16] A. T. M. Kotb, M. A. A. Nawar, Y. A. Attai, and M. H. Mohamed, "Smart optimization algorithms to enhance an axial turbine performance for wave energy conversion," *Ocean Eng.*, vol. 291, p. 116446, Jan. 2024, doi: 10.1016/j.oceaneng.2023.116446.

[17] A. T. M. Kotb, M. A. A. Nawar, Y. A. Attai, and M. H. Mohamed, "Impact of tapered leading-edge micro-cylinder on the performance of wells turbine for wave energy conversion: CFD-optimization algorithms coupling study," *Energy*, vol. 293, p. 130648, Apr. 2024, doi: 10.1016/j.energy.2024.130648.

[18] M. N. Uddin, M. Atkinson, and F. Opoku, "CFD Investigation of a Hybrid Wells Turbine with Passive Flow Control," *Energies*, vol. 16, no. 9, p. 3851, Apr. 2023, doi: 10.3390/en16093851.

[19] R. Wang, Y. Cui, Z. Liu, B. Li, and Y. Zhang, "Numerical study on unsteady performance of a Wells turbine under irregular wave conditions," *Renew. Energy*, vol. 225, p. 120255, May 2024, doi: 10.1016/j.renene.2024.120255.

[20] M. Torresi, M. Stefanizzi, L. Gurnari, P. G. F. Filianoti, and S. M. Camporeale, "Experimental characterization of the unsteady performance behavior of a Wells turbine operating at high flow rate coefficients," *E3S Web Conf.*, vol. 197, p. 08009, 2020, doi: 10.1051/e3sconf/202019708009.

[21] F. Licheri, T. Ghisu, F. Cambuli, and P. Puddu, "Experimental Analysis of the Three Dimensional Flow in a Wells Turbine Rotor," *Int. J. Turbomach. Propuls. Power*, vol. 8, no. 3, p. 21, Jul. 2023, doi: 10.3390/ijtpp8030021.

[22] A. S. Alkhalifa, M. N. Uddin, and M. Atkinson, "Aerodynamic Performance Analysis of Trailing Edge Serrations on a Wells Turbine," *Energies*, vol. 15, no. 23, p. 9075, Nov. 2022, doi: 10.3390/en15239075.

[23] B. E. Launder and D. B. Spalding, "THE NUMERICAL COMPUTATION OF TURBULENT FLOWS," in *Numerical Prediction of Flow, Heat Transfer, Turbulence and Combustion*, Elsevier, 1983, pp. 96–116. doi: 10.1016/B978-0-08-030937-8.50016-7.

[24] F. R. Menter, "Improved two-equation k-omega turbulence models for aerodynamic flows," 1992.

[25] A. Hellsten, "Some improvements in Menter's k-omega SST turbulence model," in *29th AIAA, Fluid Dynamics Conference*, Albuquerque,NM,U.S.A.: American Institute of Aeronautics and Astronautics, Jun. 1998. doi: 10.2514/6.1998-2554.

[26] A. T. M. Kotb, M. A. A. Nawar, Y. A. Attai, and M. H. Mohamed, "Performance enhancement of a Wells turbine using CFD-optimization algorithms coupling," *Energy*, vol. 282, p. 128962, Nov. 2023, doi: 10.1016/j.energy.2023.128962.